

Density and geometry of excitations in supercooled liquids up to the activation energy

Wencheng Ji,¹ Massimo Pica Ciamarra,^{2,3,*} and Matthieu Wyart^{4,†}

¹*Department of Physics of Complex Systems, Weizmann Institute of Science, Rehovot, 234 Hertzl St., Israel*

²*Division of Physics and Applied Physics, School of Physical and Mathematical Sciences, Nanyang Technological University, 21 Nanyang Link, 637371, Singapore*

³*Consiglio Nazionale delle Ricerche, CNR-SPIN, Napoli, I-80126, Italy*

⁴*Institute of Physics, École Polytechnique Fédérale de Lausanne, Lausanne, CH-1015, Switzerland*

We introduce an algorithm to uncover the activated particle rearrangements, or excitations, regulating structural relaxation in glasses at much higher energies than previously achieved. We use it to investigate the density and geometric properties of excitations in a model system. We find that the density of excitations behaves as a shifted power-law, and confirm that this shift accounts for the increase in the activation energy controlling the relaxation dynamics. Remarkably, we find that excitations comprise a core whose properties, including the displacement of the particle moving the most, scale as a power-law of their activation energy and do not depend on temperature. Excitations also present an outer deformation field that depends on the material stability and, hence, on temperature. Our analysis suggests that while excitations suppress the transition of dynamical arrest predicted by mean-field theories, they are strongly influenced by it.

In low-temperature glasses, elementary excitations are two-level systems, groups of particles that can tunnel between two states [1–6]. At much higher temperatures near the glass transition T_g , structural relaxation occurs on a time scale $\tau = \tau_0 \exp(E_a/T)$, where τ_0 is microscopic time and E_a is an activation energy that grows on cooling in fragile liquids [7]. Thermally activated local rearrangements of a few particles are important in this temperature range as well, as they contribute to structural relaxation [8–11]. Such rearrangements thus play a vital role in theories of the glass transition [12–15]. In Kinetically Constrained Models, local rearrangements are defects that can diffuse and interact to relax the system [16, 17]. In mean field theories, local rearrangements correspond to the string-like [18–21] ‘hopping processes’ through which finite-dimensional systems relax below the dynamical or mode coupling temperature T_c , where the dynamics would halt in infinite dimensions where these processes are absent [22, 23]. Finally, in elastic models of the glass transition [24–28], the energy of local excitations directly determines the activation energy E_a . Theoretically, distinct ideas have been proposed to understand the geometry of local rearrangements, including entropic considerations [29] or the existence of defects around a hexatic phase in two dimensions [17]. Alternatively, building on the notion of a length scale diverging [30–32] at the dynamical transition T_c , Ref [33] derived relationships between geometric and energetic properties of the excitations with the minimal energy.

Differentiating between different scenarios for the geometry of these excitations requires measuring their density of states $N(E)$ and geometry across a broad energy spectrum, a challenge that remains unresolved. Indeed, potential energy landscape studies [34, 35] access the consecutive excitations activated in a liquid during its relations but cannot provide the density of states of excitations. Studies conducted on the few lowest-energy excita-

tions [6, 36–39], are pertinent to the plastic and quantum properties of glasses and not directly relevant to the glass transition, which typically involves much higher energy rearrangements. We recently developed SEER [40], an algorithm based on thermal exploration that allowed us to measure $N(E)$, albeit only for energy notably smaller than the activation energy E_a . However, this study did not consider the geometry of excitations. Moreover, excitations with activation energy up to $T \log(\tau/\tau_0)$ have a significant probability to be triggered dynamically, and can then act as transition states enabling relaxation [34]. The excitations’ density of state and geometric properties in such a broad energy range have yet to be studied.

In this Letter, we perform such a study by introducing an algorithm to identify excitations via mechanical perturbations. This algorithm offers fast computation and enables access to a wide range of energies, surpassing the activation energy of the model under consideration. Our findings reveal two key insights: (i) We observe that the density of states $N(E)$ approximately follows $N(E) \propto (E - E_g(T))^a$ up to the activation energy. Additionally, we confirm that the variation in $E_g(T)$ predicts the change in activation energy [40]. (ii) Remarkably, certain geometric properties, such as the displacement δ of the most-moving particle or the probability of displaying string-like motion, only depend on their energy E . However, other properties, like the volume of an excitation, depend on both energy and temperature. We reconcile these observations by considering that excitations possess a core solely governed by their energy, which then influences the surrounding medium on a scale determined by material stability and, consequently, temperature. Overall, our results suggest that the hopping processes that suppress the mean-field dynamical transition are very much affected by it.

ASEER – We propose an athermal algorithm, the Athermal Systematic Excitation ExtRaction or

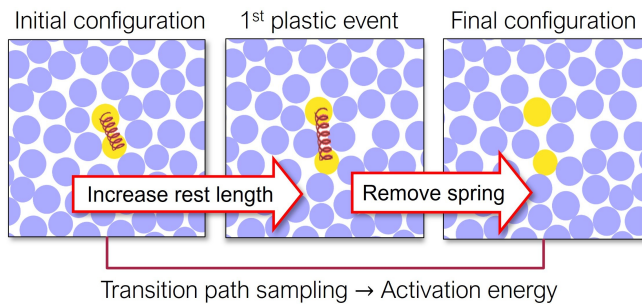


Figure 1. Illustration of the ASEER algorithm. We detect excitations by enforcing a dipolar force through a spring connecting adjacent particles of energy-minimized configurations. We gradually increase the spring rest length until an instability occurs. We then remove the spring and minimize the energy, bringing the system to a novel energy minimum. The minimum energy pathway going from one state to the other is analyzed in the absence of the spring.

‘ASEER’, to uncover the excitations associated with a reference inherent structure (IS_0). This protocol builds on the idea that changing the topology of the Voronoi neighbors induces an excitation, in analogy with the triggering of T1 transition in two spatial dimensions, see e.g. Ref. [27, 28, 41]. To uncover an excitation, we increase the separation between two adjacent (à la Voronoi) particles i and j by modifying the energy functional via the addition of an elastic spring, $E_{\text{spring}}(\Delta r) = k[(r_{ij}^0 + \Delta r) - r_{ij}^0]^2$, r_{ij}^0 being the distance between the particles in IS_0 . We have checked that the value of k is not critical and empirically fix it so that the spring is never compressed by more than 5%. We slowly increase Δr while continuously minimizing the energy to keep the system in a minimum of the expanded energy functional $U(\{\mathbf{r}_i\}) + E_{\text{spring}}(\Delta r)$. The Δr dependence of the spring energy (or of the total one) comprises smooth elastic branches punctuated by sudden drops corresponding to irreversible rearrangements. We focus on the first plastic event identified via a standard thresholding approach. When this event occurs, we remove the spring and minimize the energy again, potentially leading the system to a new IS^* . This approach is illustrated in Fig.1 and involves constraining one degree of freedom. We investigate the minimum energy path connecting IS_0 , and each uncovered IS^* via the nudge-elastic-band (NEB) method [42] to estimate the energy E_{Saddle} of the saddle point separating the considered ISs. If not stated otherwise, when the minimum energy path traverses additional ISs ($\simeq 20\%$ of cases in the considered system), we redefine IS^* as the first encountered IS and repeat the NEB analysis. This results in a catalog of unique (we ensure each IS^* appears once) excitations, each characterized by its energy barrier $E = E_{\text{Saddle}} - E_{IS_0}$ and displacement field \mathbf{dr} . This algorithm leads to large catalogs of excitations, as it uncovers from 1.2 to 2 excitations

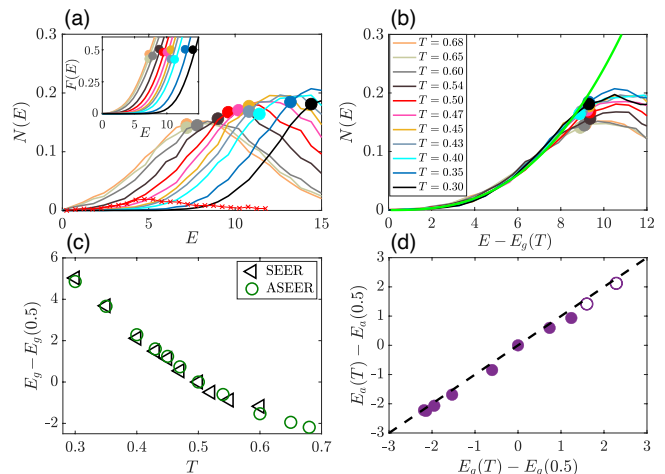


Figure 2. (a) Density of excitations $N(E)$, normalized by the system size \mathcal{N} , and its cumulative distribution $F(E)$ (inset). The solid dots mark the values of the activation energy [40], $E_a(T) = T \log(\tau/\tau_0)$, and the cross-shaped line has been obtained with the SEER algorithm at $T = 0.5$. (b) The $N(E)$ curves collapse when the energy is shifted by $E_g(T)$. The thick green curves is $N(E) \approx g_1 \times (E - E_g)^{2.7 \pm 0.1}$, where $g_1 = (4.5 \pm 0.5) \times 10^{-4}$. (c) The shift of E_g on cooling matches the shift in activation energy evaluated via SEER [40]. (d) The increase in E_g matches the increase in activation energy measured from the relaxation dynamics, with $T = 0.5$ an arbitrary reference temperature.

per particle on cooling. As demonstrated below, at low energies, ASEER matches previous algorithms systematically searching excitations via thermal fluctuations, while it performs much better at energies of the order of the activation energy E_a .

Density of states – We applied ASEER to a polydisperse three-dimensional system of $N = 2000$ soft repulsive particles [43] that can be equilibrated up to experimentally comparable temperatures through the ‘swap’ algorithm [44–47]. In recent work [40], we determined this model’s relaxation time $\tau(T)$ and microscopic timescale τ_0 , and hence the temperature dependence of its activation energy, $E_a(T) = T \log(\tau/\tau_0)$. In the Supplemental Material (SM) [48], we provide numerical details on the numerical model and the measure of the relaxation time.

Fig. 2(a) illustrates the energy E dependence of the density of excitations $N(E)$, and its cumulative $F(E)$ (inset). At each temperature T , we average over ten samples. Notably, $N(E)$ and $F(E)$ approximately shifts towards higher energy values as T decreases: the energy of local barriers grows under cooling. Indeed, before its maximum $N(E)$ is well-described by:

$$N(E) \propto (E - E_g(T))^a. \quad (1)$$

with $a \approx 2.7$, as demonstrated by the data collapse in Fig. 2(b). The characteristic energy gap E_g characterizing the system’s stability increases on cooling, as shown

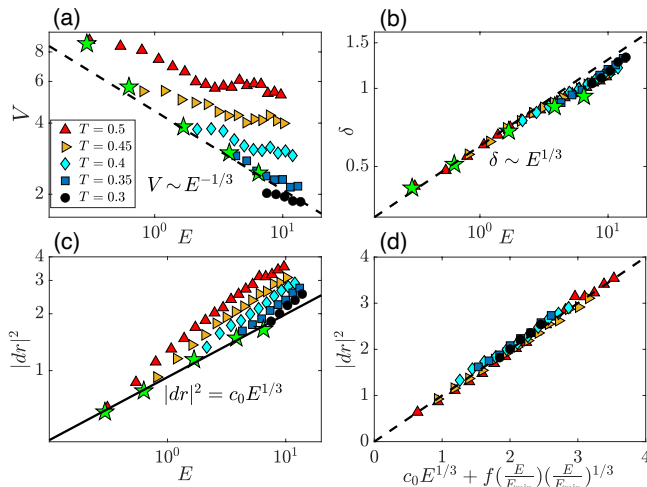


Figure 3. Dependence of (a) volume, (b) largest particle displacement, and (c) squared norm of the displacement field on the excitation’s activation energy, for various temperatures. The green stars refer to the excitations with the smallest activation energy. In all panels, we plot median values (see Fig. S2 in [48] for mean values). (d) The data in (c) are collapsed by a model postulating that the excitation core induces a T -dependent far-field displacement.

in Fig. 2(c). Fig. 2(d) shows that the variation of E_g on cooling is consistent with that of the activation energy, indicating that local barriers control the dynamics in this liquid. For the two lowest-temperatures (open circle), E_a is extracted from values of τ estimated through the time-temperature superposition principle [40, 48, 49]. The increase of a gap E_g is reminiscent of the mean-field prediction according to which, for $T < T_c$, the density of vibrational modes is gapped up to a frequency ω_{\min} indeed increasing on cooling [50].

In Fig. 2(a) and (c), we also present data obtained previously using the SEER algorithm [40]. While both algorithms yield consistent results for the variation of E_g (and of other quantities in Fig. S1 of [48]), ASEER notably detects excitation on the scale E_a , which can be activated on the relaxation time scale. Each algorithm possesses distinct advantages: SEER, reliant on thermal cycles, uncovers excitations with the smallest E , making it ideal for obtaining accurate statistics at lower E values where $N(E)$ is limited. Conversely, the mechanical ASEER algorithm accesses a wide spectrum of activation energies. Noticing that the algorithms give consistent results in the energy range accessed by both (Fig. S1), we integrate them in the subsequent analysis to acquire high-quality statistics across a broad energy range.

Architecture of lowest-energy excitations– We analyze the geometrical properties of each excitation by its displacement field, \mathbf{dr} , focusing on: (i) the characteristic number of involved particles, estimated by the participation ratio $V \equiv NP_r = (\sum \mathbf{dr}_i^2)^2 / (\sum \mathbf{dr}_i^4)$, where the

sums run over all particles i ; (ii) the squared norm of the displacement field, $|\mathbf{dr}|^2 = \sum_i \mathbf{dr}_i^2$; (iii) the maximum particle displacement, $\delta = \max_i \|\mathbf{dr}_i\|$.

By elaborating on the mean-field scenario [30–32], Ref. [33] predicted that for the excitations with minimal energy, associated with modes near the gap:

$$V_{\min}(T) \sim \frac{1}{\delta_{\min}(T)} \sim \frac{1}{|dr_{\min}(T)|^2} \sim \frac{1}{E_{\min}(T)^{\frac{1}{3}}}. \quad (2)$$

These excitations are also associated with a length scale $\ell_{\min}(T) \sim \sqrt{V_{\min}(T)}$, which is empirically known to characterize the linear response to an imposed dipole [51, 52]. Ref. [33] verified the relationships between V_{\min} , $\delta_{\min}(T)$ and $|dr_{\min}(T)|^2$, but the activation energy E_{\min} was not measured; instead a proxy corresponding to the energy difference between the two IS was used. We validate the scaling of the excitation architecture with E_{\min} in Fig. 3(a), (b) and (c) (green stars) by investigating, at each temperature, the features of the lowest-energy excitation of 1000 systems.

Note that we exclude string-like excitations from the geometrical analysis (they are defined as excitations involving the exchange of particles; see below). In general, including them only affects results for the largest energies considered, as shown in Fig. S4 [48].

Architecture of high-energy excitations – Figure 3 illustrates our main results, how the excitations’ geometric properties depend on E and T , for $E > E_{\min}$. Panel (b) shows a remarkable result: the largest displacement in an excitation depends on the excitation energy but not on its temperature so that $\delta \propto E^{1/3}$. By contrast, panels (a) and (c) demonstrate that, at fixed energy, the volume of an excitation and its squared norm increase with temperature. These facts can be visualized by considering the two-dimensional projection of the displacement field of excitations of similar energy $E \approx 10$ in systems having different temperatures, $T = 0.3$ and $T = 0.5$. Fig. 4 (a) and (b) show that these excitations have a comparable maximal magnitude at their center, but differ in the far field.

We rationalize these observations by assuming that excitations consist of (i) a core that depends only on energy E and (ii) a far-field elastic response triggered by the core. In this view, the norm square of an excitation consists of two parts $|dr|^2(T, E) = |dr|_{\text{core}}^2 + |dr|_{\text{f.f.}}^2$, which we now estimate.

Assumption (i) implies that the core is the same if $E = E_{\min}$ or $E > E_{\min}$, as long as the energy is the same. Together with Eq. 2, it thus leads to a maximal displacement of the core, and therefore of the whole excitation, behaving as $\delta \sim E^{1/3}$ and a square norm of the core $|dr|_{\text{core}}^2(E) \propto \delta^2(E)V(E) = c_0 E^{1/3}$.

If $E \gg E_{\min}$, we expect this core to act as a local strain, which generically triggers a dipolar linear elastic response in the far field [53]. It is known that the response to a unit dipole is more extended at large rather

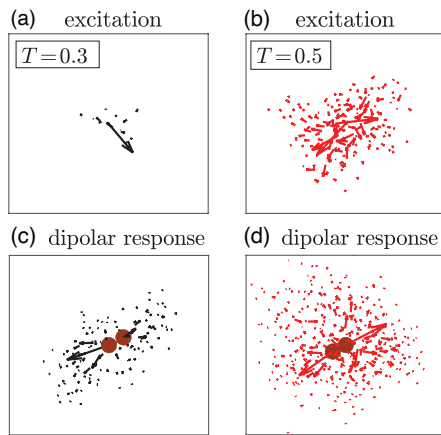


Figure 4. Representative 2D-projections of the displacement fields of excitations $E \approx 10$ and $\delta \approx 1$ at temperatures $T = 0.3$ (a) and $T = 0.5$ (b). The displacement fields are scaled by a factor of three for visualization purposes. Response fields induced by a dipole force acting on neighboring particles (brown dots) at $T = 0.3$ (c) and $T = 0.5$ (d).

than small temperatures [51, 52], as we explicitly show in Fig. 4 (c) and (d). Quantitatively, following [33, 51] we expect the volume of a unit dipole response to vary with temperature as $V_{\min}(T)$, of order $\sim E_{\min}(T)^{-1/3}$ according to Eq. 2. Moreover, we expect the norm of the dipole response to be proportional to the norm of the core itself. Putting these two effects together, we obtain $|dr|_{\text{f.f.}}^2 \propto f(E/E_{\min})|dr|_{\text{core}}^2(E)V_{\min}(T) \propto f(E/E_{\min})(E/E_{\min})^{1/3}$. Here the function $f(x)$, with $f(1) = 0$ and $\lim_{x \rightarrow \infty} f(x) = C > 0$, accounts for the fact that only high-energy excitations ($E \gg E_{\min}$) produce a far-field response that differs from the core. Overall, we find:

$$|dr|^2(T, E) = c_0 E^{1/3} + f\left(\frac{E}{E_{\min}}\right) \left(\frac{E}{E_{\min}}\right)^{1/3}. \quad (3)$$

Fig. 3(d) validates this theoretical prediction for a natural choice of interpolating function $f(x) \propto (x-1)/(x+1)$. In Fig. S3 of SM, we show that Eq. 3 also holds if E_{\min} is replaced by E_5, E_{10} (respectively the median of the five or ten lowest energy excitation) or E_g .

String-like excitations (SLEs) – Numerical simulations [39, 54, 55] and recent experiments [56] show string-like particle motion in low-temperature structural relaxation. String-like rearrangements involve one or more particles swapping positions in the excitation core, with displacements comparable to inter-particle separation [33]. We thus expect that (i) High-energy excitations are more likely string-like due to their larger displacements. (ii) The probability of a string-like excitation is T -independent as the core properties are T -independent.

We identify SLEs by assuming that particle i ends up in the position originally occupied by particle $j \neq i$ if $|\mathbf{r}_j^* - \mathbf{r}_i^0| < \Delta$, \mathbf{r}_i^0 and \mathbf{r}_j^* being the positions in the initial

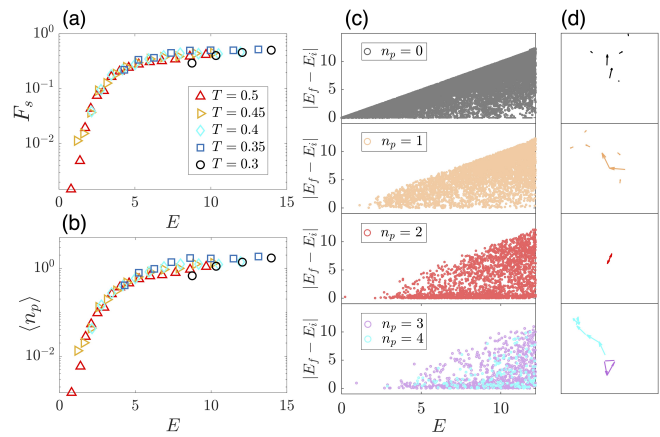


Figure 5. Energy dependence of (a) the fraction of string-like excitations and (b) the average string length, n_p . (c) Scatter plots of the energy difference between the final and initial inherent structures (ISs) versus E , for various n_p . (d) Projection of displacement fields for representative excitations onto a 2D plane. We illustrate the emergence of a string as the system moves along its minimum energy path in Animation 1 [48].

and final configurations. The choice of Δ is not critical as long as its value corresponds to a small fraction of the inter-particle distance. Here, we fix $\Delta = 0.1$. The number of particles involved in a string defines a string length $n_p = \sum_i \sum_{j, j \neq i} \theta(0.1 - |\mathbf{r}_j^* - \mathbf{r}_i^0|)$. An excitation is string-like provided $n_p \geq 1$. An example string-like excitation is in Animation 1 [48]. Fig. (5)(a) shows that an excitation is a string with a T -independent probability $F_s = \langle \theta(n_p - 1) \rangle$ that increases with E , consistently with our expectations. The string length similarly increases with E and is approximately T -independent, as we illustrate in Fig. (5)(b).

We delve deeper into the dependence of an excitation's spatial and energetic properties on the string length. Figure (5)(c) demonstrates how the energy change $|E_f - E_i|$ between the initial and final inherent structures varies with E , considering strings of different lengths at $T = 0.4$. Notably, only a few excitations with $n_p = 0, 1$ exhibit $|E_f - E_i| \simeq 0$, while this trend becomes more prevalent for larger n_p , particularly for $n_p = 2$. This phenomenon arises because many excitations with greater n_p correspond to closed strings, as depicted in Fig. (5)(d), and consequently have minimal impact on the system's structure and energy. By promoting particle motion without inducing substantial structural relaxation, these closed strings may also contribute to the breakdown of the Stokes-Einstein relation in deeply supercooled liquids, in addition to dynamical heterogeneities [57].

Discussion – Through the novel ASEER algorithm, we have measured the density of excitations in a model glass-former up to the activation energy. Our findings confirm a shift in this density under cooling that can predict the

fragility of the liquid. Most importantly, we have demonstrated that the geometry of excitations depends on both their energy and temperature, which in turn governs the stability of the overall medium. Excitations display a core whose properties scale with their energy and a far field component whose length scale is governed by temperature. These insights align with known observations on the geometry of relaxation in liquids, such as the increased predominance of strings under cooling.

These results support the idea that excitations are influenced by a dynamical transition. On one hand, the shift in the density of excitations mirrors the shift in the Hessian of the energy landscape predicted in high dimensions. This shift differs from a simple rescaling, as one might expect from a naive interpretation of elastic models where energies are scaled by a temperature-dependent elastic modulus. On the other hand, the excitation core follows scaling laws expected in the vicinity of a dynamical transition. According to this perspective, hopping processes suppress the divergence of the relaxation time at T_c but are very much influenced by the elastic instability associated with T_c .

Acknowledgments: We thank the Simons collaboration and L. Berthier, G. Biroli, C. Brito, C. Gavazzoni, E. Lerner, M. Muller, M. Popovic, M. Ozawa and A. Tahaei for discussions. M.P.C. discloses support for the research of this work from Singapore Ministry of Education [MOE-T2EP50221-0016]. M.W acknowledges support from the Simons Foundation Grant (No. 454953 Matthieu Wyart) and from the SNSF under Grant No. 200021-165509.

* massimo@ntu.edu.sg

† matthieu.wyart@epfl.ch

- [1] W. Phillips, *J. Low Temp. Phys.* **7**, 351 (1972).
- [2] P. Anderson, B. Halperin, and C. Varma, *Philos. Mag.* **25**, 1 (1972).
- [3] W. A. Phillips, *Reports on Progress in Physics* **50**, 1657–1708 (1987).
- [4] D. Queen, X. Liu, J. Karel, T. Metcalf, and F. Hellman, *Physical review letters* **110**, 135901 (2013).
- [5] T. Pérez-Castañeda, C. Rodríguez-Tinoco, J. Rodríguez-Viejo, and M. Ramos, *Proc. Natl. Acad. Sci.* **111**, 11275 (2014).
- [6] D. Khomenko, C. Scalliet, L. Berthier, D. Reichman, and F. Zamponi, *Phys. Rev. Lett.* **124**, 225901 (2020).
- [7] C. Angell, *Relaxations in complex systems*, 3 (1985).
- [8] D. S. Simmons, M. T. Cicerone, Q. Zhong, M. Tyagi, and J. F. Douglas, *Soft Matter* **8**, 11455 (2012).
- [9] M. Pica Ciamarra, R. Pastore, and A. Coniglio, *Soft Matter* **12**, 358 (2015).
- [10] M. T. Cicerone, Q. Zhong, and M. Tyagi, *Physical Review Letters* **113**, 117801 (2014).
- [11] M. T. Cicerone, K. Badilla-Nunez, J. Zahn, J. P. Stoppelman, and J. G. McDaniel, (2023), [arXiv:2201.12593](https://arxiv.org/abs/2201.12593).
- [12] D. L. Anderson, *Science* **267**, 1618–1618 (1995).
- [13] P. G. Debenedetti and F. H. Stillinger, *Nature* **410**, 259–267 (2001).
- [14] J. C. Dyre, *The Journal of Physical Chemistry Letters* **15**, 1603–1617 (2024).
- [15] L. Berthier, E. Flenner, C. Fullerton, C. Scalliet, and M. Singh, *J. Stat. Mech. Theory Exp.* **2019**, 064004 (2019).
- [16] J. P. Garrahan and D. Chandler, *Physical Review Letters* **89** (2002).
- [17] D. Fraggedakis, M. R. Hasyim, and K. K. Mandadapu, *Proceedings of the National Academy of Sciences* **120** (2023).
- [18] W. Gotze and L. Sjogren, *Journal of Physics C: Solid State Physics* **21**, 3407 (1988).
- [19] K. S. Schweizer and E. J. Saltzman, *The Journal of Chemical Physics* **119**, 1181–1196 (2003).
- [20] K. Vollmayr-Lee, W. Kob, K. Binder, and A. Zippelius, *The Journal of chemical physics* **116**, 5158 (2002).
- [21] P. Charbonneau, Y. Jin, G. Parisi, and F. Zamponi, *Proceedings of the National Academy of Sciences* **111**, 15025–15030 (2014).
- [22] V. Lubchenko and P. Wolynes, *Phys. Rev. Lett.* **87**, 195901 (2001).
- [23] G. Biroli and J.-P. Bouchaud, *Structural Glasses and Supercooled Liquids: Theory, Experiment, and Applications*, 31 (2012).
- [24] J. Dyre, *Rev. Mod. Phys.* **78**, 953 (2006).
- [25] C. Rainone, E. Bouchbinder, and E. Lerner, *Proceedings of the National Academy of Sciences* **117**, 5228 (2020).
- [26] G. Kapteijns, D. Richard, E. Bouchbinder, T. B. Schröder, J. C. Dyre, and E. Lerner, *The Journal of Chemical Physics* **155**, 74502 (2021).
- [27] Y.-W. Li, Y. Yao, and M. P. Ciamarra, *Physical Review Letters* **128**, 258001 (2022).
- [28] M. Lerbinger, A. Barbot, D. Vandembroucq, and S. Patinet, *Physical Review Letters* **129**, 195501 (2022).
- [29] J. Stevenson and P. Wolynes, *Nat. Phys.* **6**, 62 (2010).
- [30] S. Franz and G. Parisi, *J. Phys. Condens. Matter* **12**, 6335 (2000).
- [31] G. Biroli, J.-P. Bouchaud, K. Miyazaki, and D. Reichman, *Phys. Rev. Lett.* **97**, 195701 (2006).
- [32] S. Franz, G. Parisi, F. Ricci-Tersenghi, and T. Rizzo, *Eur. Phys. J. E* **34**, 1 (2011).
- [33] W. Ji, T. W. de Geus, E. Agoritsas, and M. Wyart, *Physical Review E* **105**, 044601 (2022).
- [34] B. Doliwa and A. Heuer, *Physical Review Letters* **91**, 235501 (2003).
- [35] A. Heuer, *J. Phys. Condens. Matter* **20**, 373101 (2008).
- [36] W. Ji, M. Popović, T. de Geus, E. Lerner, and M. Wyart, *Phys. Rev. E* **99**, 023003 (2019).
- [37] H. Schober, C. Oligschleger, and B. Laird, *J. Non. Cryst. Solids* **156-158**, 965 (1993).
- [38] L. Wang, A. Ninarello, P. Guan, L. Berthier, G. Szamel, and E. Flenner, *Nat. Commun.* **10**, 26 (2019).
- [39] W. Ji, T. de Geus, M. Popović, E. Agoritsas, and M. Wyart, *Phys. Rev. E* **102**, 062110 (2020).
- [40] M. P. Ciamarra, W. Ji, and M. Wyart, (2023), [10.48550/arXiv:2302.05150](https://arxiv.org/abs/10.48550/arXiv:2302.05150).
- [41] M. Popović, V. Druelle, N. A. Dye, F. Jülicher, and M. Wyart, *New Journal of Physics* **23**, 033004 (2021).
- [42] N. A. Zarkevich and D. D. Johnson, *The Journal of Chemical Physics* **142**, 24106 (2015).
- [43] E. Lerner, *J. Non-Cryst. Solids* **522**, 119570 (2019).
- [44] J. Briano and E. Glandt, *J. Chem. Phys.* **80**, 3336 (1984).

- [45] R. Gutiérrez, S. Karmakar, Y. Pollack, and I. Procaccia, *Europhys. Lett.* **111**, 56009 (2015).
- [46] A. Ninarello, L. Berthier, and D. Coslovich, *Phys. Rev. X* **7**, 021039 (2017).
- [47] C. Brito, E. Lerner, and M. Wyart, *Phys. Rev. X* **8**, 031050 (2018).
- [48] See Supplemental Material at <http://...> for additional figures..
- [49] L. Berthier and M. D. Ediger, *The Journal of Chemical Physics* **153**, 44501 (2020).
- [50] T. Castellani and A. Cavagna, *Journal of Statistical Mechanics: Theory and Experiment* **2005**, P05012 (2005).
- [51] E. Lerner, E. DeGiuli, G. Düring, and M. Wyart, *Soft Matter* **10**, 5085 (2014).
- [52] C. Rainone, E. Bouchbinder, and E. Lerner, *Proc. Natl. Acad. Sci.* **117**, 5228 (2020).
- [53] G. Picard, A. Ajdari, F. Lequeux, and L. Bocquet, *Phys. Rev. E* **71**, 010501 (2005).
- [54] C. Donati, J. Douglas, W. Kob, S. Plimpton, P. Poole, and S. Glotzer, *Phys. Rev. Lett.* **80**, 2338 (1998).
- [55] H.-B. Yu, R. Richert, and K. Samwer, *Sci. Adv.* **3**, e1701577 (2017).
- [56] Y. Chen, Z. Ye, K. Wang, J. Huang, H. Tong, Y. Jin, K. Chen, H. Tanaka, and P. Tan, *Nature Physics* **19**, 969–977 (2023).
- [57] M. D. Ediger, *Annual review of physical chemistry* **51**, 99 (2000).
-

Supplementary Material for Density and geometry of excitations in supercooled liquids up to the activation energy

Numerical model, relaxation dynamics and activation energy

We consider a three-dimensional system of soft repulsive particles [43] with size σ distributed as $p(\sigma) \propto \sigma^{-3}$ in the range $[\sigma_{\min}; 2.2\sigma_{\min}]$. This modern numerical model can be equilibrated up to experimentally comparable temperatures through the ‘swap’ algorithm [44–47]. The pair interaction is given by

$$U(r_{ij}) = \epsilon \left[\left(\frac{\sigma_{ij}}{r_{ij}} \right)^{10} + \sum_{l=0}^3 c_{2l} \left(\frac{r_{ij}}{\sigma_{ij}} \right)^{2l} \right] \quad (4)$$

for $r_{ij} < x_c = 1.4$. We use a non-additive particle size $\sigma_{ij} = \frac{1}{2}(\sigma_i + \sigma_j)(1 - 0.1|\sigma_i - \sigma_j|)$ to prevent crystallization and set c_{2l} to enforce continuity at x_c up to three derivatives. We studied systems of $\mathcal{N} = 2000$ particles of mass m at number density $\rho = 0.58$ in cubic simulation boxes with periodic boundary conditions. We express mass in units of m , temperature in units of ϵ , lengths in units $\rho^{-1/3}$, and time in units of $\sqrt{m\sigma_{\min}^2/\epsilon}$. We minimize the energy of configurations equilibrated at temperature T to produce ISs that we investigate with ASEER.

For this model system, in a previous work [40], we have (i) investigated the relaxation dynamics and shown that the self-scattering correlation function evaluated at the first peak of the static structure factor, a self-overlap function, and a total-overlap function, give consistent measures for the temperature dependence of the relaxation time τ . All correlation functions satisfy the time-temperature superposition principle, which we exploit to measure the relaxation time at very low temperatures. (ii) estimated the microscopic time τ_0 influencing the relaxation time, $\tau = \tau_0 e^{E_a(T)/T}$.

The evaluation of τ and of τ_0 allows us to measure the activation energy regulating structural relaxation, $E_a(T) = T \log(\tau/\tau_0)$. $E_a(T)$ fixes the scale of the activation energy of the excitations that have a non-negligible probability of being activated during the relaxation dynamics. The ASEER algorithm crucially allows us to extract excitations with activation energy up and beyond E_a .

Consistency between SEER and ASEER

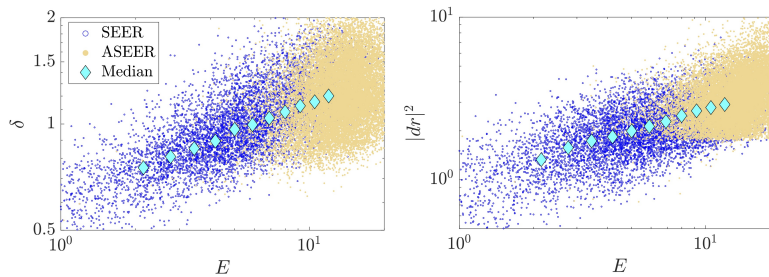


Figure S1. We have shown in Fig. 2a that SEER and ASEER give consistent results for the density of excitations $N(E)$ in the energy range they both access. The E dependence of δ and $|dr|^2$ further confirms the consistency of these methods. We also illustrate median values (in cyan) at different E up to E_a , as shown in Fig. 3 in the main text. Data refer to $T = 0.4$.

Median and mean values satisfy the scaling relations

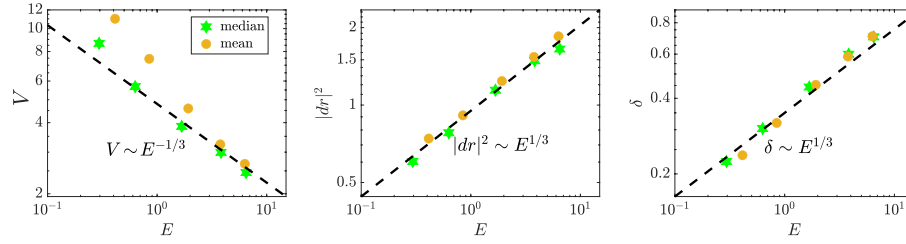


Figure S2. In the main text, we have verified the scaling relations Eq. 3 by focusing on the median values of $V = NP_r$, $|dr|^2$, δ , for the lowest energy excitations across 1000 samples. We show in these figures that the mean values behave analogously.

Robustness of Eq. 4 with respect to the definition of E_{\min}

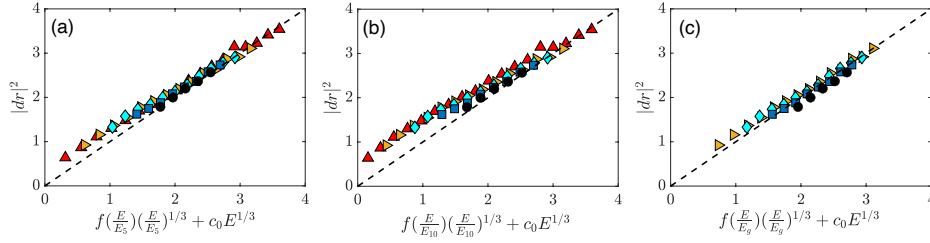


Figure S3. We validated our proposed functional form (Eq. 4) for $|dr|^2(T, E) = |dr|^2(E_{\min}(T), E)$ by adopting for E_{\min} the median value of the lowest-energy excitations across 1000 independent samples. We prove the robustness of our prediction by showing that a data collapse is also obtained by replacing E_{\min} with the median of the five lowest excitations E_5 (a), the median of the ten lowest excitations E_{10} (b), or the gap energy E_g (c).

Architecture of high-energy excitations: the role of string-like excitations

Fig. 3 in the main text investigated the architecture of high-energy excitations that are not string-like. Including strings as well leave our results unchanged at small and intermediate energies. At very large energies, strings dominate and corrections are apparent for V and δ , and less so $|dr|^2$.

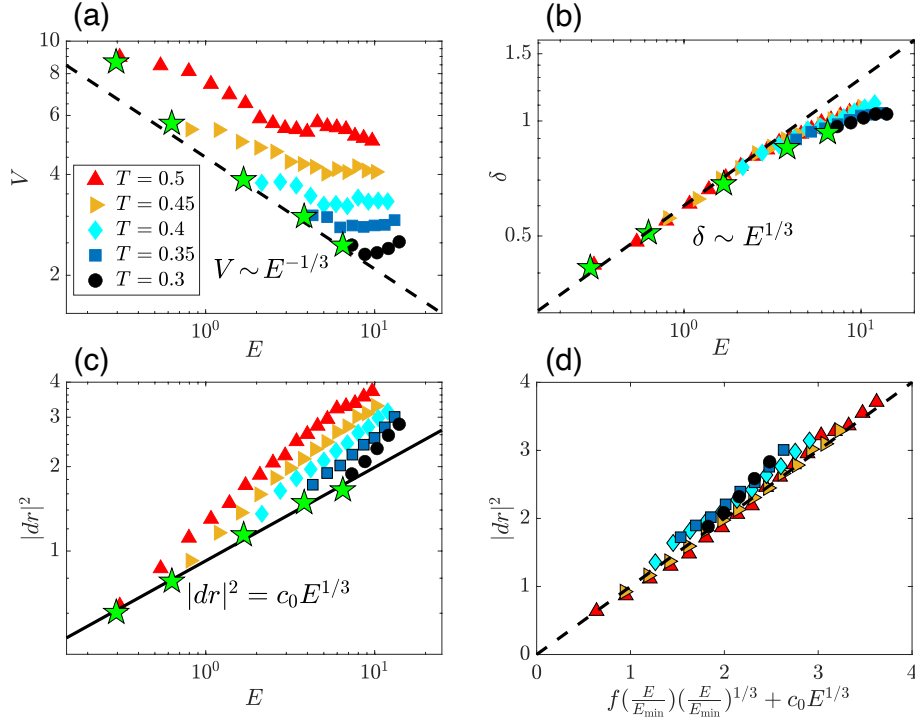


Figure S4. The analysis of the geometrical properties of non-string-like excitations illustrated in Fig. 3 in the main text is here repeated by also considering them.